Age and Gender Related Changes in the Normal Human Brain using Hybrid Diffusion Imaging (HYDI)

Yu-Chien Wu[a,b,c], **Aaron S. Field**[a,d], **Paul J. Whalen**[c,e], and **Andrew L. Alexander**[b,f,g]

[a]Department of Radiology, University of Wisconsin-Madison, Madison, WI, USA

[b]Waisman Laboratory for Brain Imaging and Behavior, University of Wisconsin-Madison, Madison, WI, USA

[c]Dartmouth Brain Imaging Center, Dartmouth College, Hanover, NH, USA

[d]Department of Biomedical Engineering, University of Wisconsin-Madison, Madison, WI, USA

[e]Department of Psychological and Brain Sciences, Dartmouth College, Hanover, NH, USA

[f]Department of Medical Physics, University of Wisconsin-Madison, Madison, WI, USA

[g]Department of Psychiatry, University of Wisconsin-Madison, Madison, WI, USA

Abstract

Diffusion tensor imaging has been widely used to study brain diseases, disorders, development and aging. However, few studies have explored the effects of aging on diffusion imaging measures with higher b-values. Further the water diffusion in biological tissues appears bi-exponential although this also has not been explored with aging. In this study, hybrid diffusion imaging (HYDI) was used to study fifty-two healthy subjects with an age range from 18 to 72 years. The HYDI diffusion-encoding scheme consisted of five concentric q-space shells with b-values raging from 0 to 9375 s/mm^2. Quantitative diffusion measures were investigated as a function of age and gender using both region-of-interest (whole brain white matter, genu and splenium of corpus callosum, posterior limb of the internal capsule) and whole-brain voxel based analyses. Diffusion measures included measures of the diffusion probability density function (zero displacement probability, and mean squared displacement), bi-exponential diffusion (i.e. volume fractions of fast/slow diffusion compartments and fast/slow diffusivities), and DTI measures (fractional anisotropy, mean diffusivity, axial diffusivity and radial diffusivity). The bi-exponential volume fraction, the fast diffusivity, and the axial diffusivity measures (f1, D1 and Da) were found to be more sensitive to normal aging than the restricted, slow and radial diffusion measures (Po, D2 and Dr). The bi-exponential volume fraction, f1, showed the most widespread age-dependence in the voxel-based analyses although both FA and mean diffusivity did show changes in frontal white matter regions that may be associated with age-related decline.

Correspondence to: Yu-Chien Wu, Dartmouth Brain Imaging Center, 6207 Moore Hall Hanover, NH. 03755 Tel: (603) 646-2909, Fax: (603) 646-1419 Yu-Chien.Wu@Dartmouth.edu.

Keywords

diffusion weighted imaging; diffusion tensor imaging; diffusion spectrum imaging; bi-exponential diffusion; age; gender

Introduction

Diffusion tensor imaging (DTI) is widely used to characterize water diffusion and microstructure in biological tissues, particularly in the brain (Basser et al., 1994). DTI uses a simple, 3D, multivariate Gaussian model to describe the diffusion behavior of water molecules in biological substrates (Basser and Pierpaoli, 1996). In fibrous or organized tissue like cerebral white matter (WM), water exhibits anisotropic diffusion behavior. From the diffusion tensor model, the tissue microstructure may be described using the fractional anisotropy (FA), the mean diffusivity (MD), the axial diffusivity (Da) and the radial diffusivity (Dr). While many WM studies using DTI have focused on FA, other measures like Da and Dr appear to be correlated with axonal integrity and myelination in WM, respectively (Song et al., 2002; Alexander et al. 2007).

Many studies have used DTI to investigate the effects of aging and/or gender on healthy adult brain tissues (Abe et al., 2002, 2008; Ardekani et al., 2007; Ben Bashat et al., 2005; Bhagat and Beaulieu, 2004; Helenius et al., 2002; Hus et al., 2008; Head et al., 2004; Hugenschmidt et al., 2008; McLaughlin et al., 2007; Pfefferbaum et al., 2000, 2005; Pfefferbaum and Sullivan, 2003; Salat et al., 2005; Szeszko et al., 2003). Despite these studies, there has been little consensus regarding age-related changes in DTI measures, except a trend of evidence supporting an anterior-posterior gradient of changes in FA and MD with age (Ardekani et al., 2007; Bhagat and Beaulieu, 2004; Head et al., 2004; Pfefferbaum et al., 2000, 2005; Pfefferbaum and Sullivan, 2003; Salat et al., 2005). In particular, FA appears to decrease with age in the WM of anterior frontal regions but is well preserved in posterior parts of normal elderly brains (Pfefferbaum et al., 2005). In contrast to FA decline, MD appears to increase with age in anterior brain regions. In addition, while most of the DTI studies focus on the changes of FA and MD, few studies (e.g., Bhagat and Beaulieu, 2004; Hsu et al., 2008) have reported changes in Da and Dr, which may reveal more tissue-specific information about normal aging.

Although DTI successfully describes the water diffusion behavior at modest b-values (e.g., 1000s/mm^2) many studies have demonstrated that simple Gaussian diffusion models do not sufficiently describe water diffusion in complex tissues – such as in areas of crossing fibers (Alexander et al., 2001; Alexander et al., 2002). Further, at high levels of diffusion-weighting, the signal does not exhibit mono-exponential decay with increasing b-values (Assaf & Cohen, 1998; Inglis et al., 2001; Maier et al., 2001; 2004; Mulkern et al., 1999). The q-space diffusion formalism described by Callaghan (Callaghan 1991) may be used to directly estimate the probability density function (PDF), i.e. the probability of water displacement function, or diffusion spectrum (Wedeen et al., 2005). This approach is model-free and more general than DTI for describing complex diffusion behavior and tissue organization. However, only one study to date has examined the changes in q-space measures with age in children and young adults (Ben Bashat et al., 2005). In that study, FA and the q-space zero-displacement probability demonstrated an increase with age (from 4 months to 23 years). Age effects on q-space measures have not been studied beyond young adulthood and this was the focus of the present study.

DWI protocols have recently been developed to characterize q-space measurements in human brains on clinical MRI scanners (Assaf et al., 2002) including the diffusion spectrum

imaging (DSI) technique (Wedeen et al., 2005). An alternative q-space encoding scheme called hybrid diffusion imaging (HYDI) was recently developed (Wu and Alexander, 2007; Wu et al., 2008), which obtains measurements on concentric spherical shells in q-space. An advantage of this q-space sampling strategy is that it facilitates multiple DWI analyses from a single HYDI data set. For example, in this study, the inner shells of the HYDI data are processed using a diffusion tensor model, and the whole q-space sample datasets are processed using DSI analysis methods and bi-exponential model fitting.

In this study, HYDI was used to investigate both q-space and DTI measures in brain tissues from 52 healthy human subjects whose ages ranged from 18 to 72 years. Age and gender effects were studied using voxel-based analysis and also with linear regression analyses on whole brain WM, and regions-of-interest (ROIs) in the corpus callosum and internal capsule. The q-space measures included PDF measures, Po (the zero displacement probability) and MSD (mean squared displacement), and measures of a bi-exponential diffusion model, f1 (the volume fraction of the fast diffusion compartment), f2 (the volume fraction of the slow diffusion compartment), D1 (averaged fast diffusivity) and D2 (averaged slow diffusivity) (Wu & Alexander, 2007). The DTI measures included FA, MD, Da and Dr. Q-space measures may provide new descriptors of tissue microstructure that are less sensitive than DTI to the effects of crossing fibers. In addition, these measures have been found to be sensitive to neuropathology, particularly WM demyelination (Assaf et al., 2002; 2005; Bar-Shir et al., 2009; Biton et al., 2006; Mayzel-Oreg et al., 2007). Therefore, it is increasingly important to understand the nature of their dependency on healthy aging beyond young adulthood.

Materials and Methods

Subjects and MRI scanning protocol

Fifty-two right-handed healthy volunteers (age: 18–72 years-old, mean 39 ± 14 years) including 29 females (43 ± 14 years old) and 23 males (34 ± 11 years old) were recruited in this study. The age distributions of females and males were not significantly different (ANOVA; $p>0.05$). Informed consent was obtained from each subject in compliance with the guidelines of the Institutional Review Board. All subjects were screened by the in-house Brain Health Checklist and the Holden Psychological Screening Inventory (HPSI) (Holden, 1996) to exclude those with abnormal pathological and psychological diseases and conditions. In addition, T1-weighted images of all subjects were reviewed by a neuroradiologist to detect any unsuspected pathology or significant structural abnormalities. Images were not screened for T2-weighted hyperintensities.

HYDI was performed on a 3.0T GE-SIGNA scanner with an 8-channel head coil and ASSET parallel imaging. The DW pulse sequence was a single-shot, spin-echo, echo-planar imaging (SS-SE-EPI) with pulse-oximeter gating. MR parameters were: TR = 10–15 heartbeats (effective TR ~ 12–15 sec), TE = 122 ms, FOV = 256 mm, matrix = 128×128, voxel size = 2×2 mm^2, 30 slices with slice thickness = 3mm, and a total scan-time of about 30 min. The HYDI encoding scheme is described in Table 1. Diffusion parameters were: maximum b-value = 9375 s/mm^2, diffusion gradient duration δ = 45 ms, diffusion gradient separation Δ = 56ms, q-space sampling interval Δq_r = 15.2mm^{-1}, maximum length of the q-space wave vector q_{max} = 76.0mm^{-1}, field of view of the diffusion displacement space FOV_R = $(1/\Delta q_r)$ = 65μm, and resolution of the diffusion displacement space ΔR = $(1/2q_{max})$ = 6.6μm (Callaghan 1991). The FOV_R describes the width of the reconstructed displacement spectrum and ΔR describes the resolution in the displacement space.

HYDI Data Processing

Measures of the diffusion probability density function (PDF), including Po (zero displacement probability) and MSD (mean squared displacement), were computed using the whole HYDI dataset. Fast and slow diffusion were computed using the whole HYDI dataset using a bi-exponential model. Measures of bi-exponential diffusion included f1 (volume fraction of the fast diffusion compartment), f2 (volume fraction of the slow diffusion compartment), D1 (averaged diffusivity of the fast diffusion compartment), and D2 (averaged diffusivity of the slow diffusion compartment). Note that the summation of f1 and f2 was constrained to 1. Details of these computations (PDF and bi-exponential fitting) are described in previous papers (Wu and Alexander 2007; Wu et al., 2008). Given that Po is the probability that water molecules minimally diffuse within the diffusion time (Δ), it is a marker of the most restricted/hindered diffusion. DTI measures (FA (fractional anisotropy), MD (mean diffusivity), Da (axial diffusivity), Dr (radial diffusivity)) were processed using the second shell of the HYDI scheme in Table 1. FA and MD were calculated using conventional definitions (Basser et al., 1994); Da is equal to the major eigenvalue (λ_1), and Dr is the average of the medium and minor eigenvalues (($\lambda_2 + \lambda_3$)/2) of the DT model (Song et al., 2002). The HYDI data processing used in-house Matlab codes as described previously (Wu et al., 2008). DTI data were processed using the CAMINO diffusion image analysis software library (Cook et al., 2006). An advantage of this approach is that all of the diffusion maps are derived from the same data and thus are inherently co-registered.

White matter (WM) probability maps were obtained from the Po maps using the FMRIB (http://www.fmrib.ox.ac.uk/fsl) automated segmentation tool, FAST, after skull stripping using BET (Zhang et al., 2001). WM masks were generated using thresholds on the probability maps to improve tissue specificity and minimize partial-volume effects. Shown in Figure 1 (a), voxels with WM probability > 0.90 were used for the following whole brain WM analyses. This probability threshold was selected to reduce partial voluming effects; however, the results were very similar for other probability thresholds down to a 0.5 level. Region-specific analyses were also performed using regions of interest (ROI) in the genu of the corpus callosum (CCg), the splenium of the corpus callosum (CCs) and the posterior limbs of the internal capsules (PLIC). An illustration of ROI locations is shown in Figure 1 (b). All ROIs were 3-dimensional and covered 4 consecutive slices. Linear regression was used to test for age and gender effects of all diffusion measures for the whole brain WM and measurements within ROIs. In addition, for both whole brain WM and ROI studies, analysis of covariance (ANCOVA) was performed to test whether age dependencies differed between genders.

Voxel-Based Analysis (VBA)

Voxel-based analysis was performed using a tissue-specific, smoothing-compensated (TSPOON) approach, which improves tissue specificity and compensates for image misregistration and smoothing (Lee et al., 2009). First, maps of all diffusion measures were segmented using a WM probability mask described in the previous section without thresholding. Next, the segmented maps of diffusion measures and the WM probability mask in the subject native space were transformed (normalized) to the standard MNI-152 (Montreal Neurological Institute, 152 subjects) space. This transformation involved template creation and a two-stage registration using FLIRT (FMRIB's image registration tool, http://www.fmrib.ox.ac.uk/fsl/flirt/) (Jenkinson and Smith, 2001).

The Po template was created in 2 stages. In the first stage, the Po image of a 26-year-old male subject was selected as an initial template. The other 51 subjects' Po maps were spatially normalized to this single subject template using a 12-parameter affine transformation and a cost function of normalized mutual information with FLIRT. The 52

normalized Po maps were averaged to create an averaged Po template. The spatial normalization procedure was then repeated using the average Po template as the target. The first stage registration was a spatial transformation between two low-resolution images – the subjects' Po maps and the averaged Po template using a 12-parameter affine transformation and a cost function of normalized mutual information. The second stage registration was a spatial transformation from the low-resolution image to the high resolution MNI space using the same transformation parameters. The averaged Po template was normalized to the MNI-152 T1-weighted 1mm resolution brain images provided by FSL (FMRIB software library). The final normalization was to apply the transform matrixes from the first and the second stage of registration to all the segmented diffusion measures and the WM probability mask.

Both the WM-segmented diffusion measure maps and the WM masks were normalized to the standard space. All normalized images (diffusion maps and masks) were smoothed with a 6-mm 3D Gaussian kernel. The segmented, normalized, and smoothed diffusion measures were then divided by the identically normalized and smoothed WM mask as described by the TSPOON approach (Lee et al., 2009). The voxel-based statistical analysis was performed using permutation testing in FSL (Nichols & Holmes, 2002) with the threshold-free cluster enhancement (TFCE) method for finding clusters (Smith & Nichols, 2009). Age and gender were treated as confound regressors and the results were thresholded at $p < 0.05$ with the family-wise error rate (FWE) correction.

Results

Representative maps of the diffusion measures from a single HYDI scan are shown in Figure 2. As presented in Figure 2 (a) and (g), both Po and FA had high tissue contrast between white matter (WM) and gray matter (GM). However, Po values in WM were more homogeneous across the whole brain compared to FA, which was hypointense at crossing fiber areas such as prefrontal WM and intersections between the optical radiation and the superior longitudinal fasiculus. Therefore, in this study Po maps were used for tissue segmentation and as the primary registration map for spatial normalization in the voxel-based analysis (VBA).

Average Diffusion Measures Across Sample

The volume fraction of the fast diffusion compartment (f1) was 1 for CSF but ranged from ~0.6 to 0.8 for WM; the volume fraction of the slow diffusion compartment ranged from ~0.2 to 0.4 for WM (Figure 2 (c)–(d) and Table 2). The averaged fast diffusivity (D1, Figure 2 (e)) was similar in both WM and GM at ~1000 $\times 10^{-6}$ s/mm^2 (Table 2), but the averaged slow diffusivity (D2, Figure 2 (f)) was much lower in the WM at ~100 $\times 10^{-6}$ s/mm^2 (Table 2). These data (f1, f2, D1 and D2) were consistent with reported data (Maier et al., 2004), but were a bit smaller than the results of (Clark et al., 2002). In Figure 2 (i) and (j), Da was highest and Dr was lowest in regions of compact WM such as the corpus callosum and internal capsules, but appeared similar to GM in WM areas that include crossing fibers. The means of the diffusion measures are listed in Table 2 for the whole brain WM and ROIs in the genu of the corpus callosum (CCg), splenium of the corpus callosum (CCs) and posterior limbs of internal capsules (PLIC).

Age Dependence in Whole-Brain White Matter and Regions of Interest

Table 3 lists statistics results of linear regression analysis of diffusion measures vs. age. Bold fonts indicate diffusion measures with significant fit ($p<0.05$). The correlations of diffusion measurements and age were described by the correlation coefficient, R. The scatter plots of DW measures vs. age and the regression lines (for $p < 0.05$) are shown in Figures 3

(WM), 4 (CCg), 5 (PLIC) and 6 (CCs). Note that f2, the volume fraction of the slow diffusion compartment, was not plotted because f2 is the complement of f1, i.e. $f2 = 1 - f1$, the regression results are identical except the sign of the slope. Significant age-related changes were observed for f1, f2, D1, Da, and Dr in whole brain WM (WBWM) and the ROIs (Table 3). The volume fraction of the fast diffusion compartment, f1, decreased with age in WBWM (Figure 3 (c)), whereas the averaged fast diffusivity (D1) increased with age in WBWM and CCs (Figure 3 (d) and Figure 6 (d)). The axial diffusivity (Da) decreased with age in WBWM and CCg (Figure 3 (h) and Figure 4(h)), while the radial diffusivity increased with age in CCg (Figure 4(i)). The coincidental decrease of Da and increase of Dr may explain the decrease of FA in CCg in Figure 4 (f). Note that although the changes in diffusion measures were significant, the relative changes per decade ($10*\beta_1$ in Table 3) were only 1–4% of their mean values (Table 2). This means that for an age difference of 50 years (roughly the time span of this study), the diffusion measures, on average, will change between 5% and 20%. Po, MSD, D2 and MD were not sensitive to age effects for WBWM or the ROIs. Of the specific regions studies, the genu of the corpus callosum (CCg) was the most sensitive anatomical structure to age effects. Conversely, the middle to posterior portions of the brain including the posterior limbs of the internal capsule (PLIC) and the splenium of the corpus callosum (CCs) did not show significant changes for any of the DW measures, except D1 of CCs with a weakly significant p-value = 0.047 (Table 3).

Gender Effects in Whole Brain White Matter and Regions of Interest

Gender effects were also tested in the linear regression analyses with male=1 and female=0. The FA of WBWM was significantly lower in females (p <0.02). Significant gender differences were not found for any of the diffusion measures in the ROIs. When age dependence was statistically significant, gender effects on the age-related changes (i.e. the slope of regression lines of age effects) were tested using ANCOVA. No significant gender differences in age dependence were detected.

Voxel-Based Analyses

The voxel-based analysis (VBA) results are summarized in Table 4 for the HYDI measures and Table 5 for the DTI measures with the maximum p-values, cluster sizes, MNI coordinates of the maximum p-values and the anatomical location of clusters. The anatomical locations were identified based on the International Consortium for Brain Mapping (ICBM)-DTI-81 white-matter labels atlas (Mori et al., 2005) and the Johns Hopkins University (JHU) white-matter tractography atlas (Hua et al., 2008) provided by the FMRIB Software Library (FSL). Statistical maps of the diffusion measures versus age are shown in Figures 7–11. Only Po, MSD, f1, FA and Da showed significant age effects, where Po and MSD increased with age (positive correlation), while f1, FA and Da decreased with age (negative correlation) (Table 4 and 5). The f1 and DTI measures (FA, Da) had the most widespread age dependence (Table 4 and 5; Figures 9–11). The regional age dependences appeared to involve more peripheral WM and less major WM tracts (e.g., corpus callosum, internal capsules and centrum semiovale) (Figures 9–11), except FA in the genu of the corpus callosum (Figure 10). Maps of significant gender effect are shown in Figure 12 for MSD, f2, D2, FA, MD and Dr. The right inferior longitudinal fasciculus in men showed increased MSD, D2 and FA, and decreased f1, MD and Dr.

Discussion

In this study, a flexible diffusion-weighted MRI method – hybrid diffusion imaging (HYDI) – was used to investigate the relationships between diffusion measures versus aging and gender in a healthy adult sample. A strength of the HYDI method is that it is well-suited for multiple types of DWI analysis including more conventional DTI, q-space or DSI, HARDI

(at a specific shell), and bi-exponential diffusion modeling. Specifically we evaluated standard DTI measures, bi-exponential diffusion measures and high b-value diffusion spectrum measures. To our knowledge this is the first study to examine either high b-value or bi-exponential diffusion measures versus age or gender in middle- aged adults. Although the data collection in this study took nearly 30 minutes, similar HYDI protocols of less than 12 minutes are possible on new MRI scanners with faster and stronger imaging gradients with higher duty cycle limits. More efficient acquisition of HYDI data will make it more amenable to clinical research studies in a broad spectrum of applications.

VBA analyses of FA revealed significant decreases with age in the genu of the corpus callosum (also in the ROI) as well as areas of prefrontal white matter and occipito-parietal white matter regions (with larger effects on the left). The decline in FA with aging has been reported in a large number of studies (Ardekani et al., 2007; Bhagat and Beaulieu, 2004; Head et al., 2004; Pfefferbaum et al., 2000, 2005; Pfefferbaum and Sullivan, 2003; Salat et al., 2005, Hsu et al., 2008; Hugenschmidt et al., 2008; Voineskos et al., 2010; Bendlin et al., in press) although there is considerable variation in the anatomical locations of FA decline. One of the more consistent regions of FA decline is the genu of the corpus callosum (Hsu et al., 2008; Voineskos et al., 2010). Several of these studies suggest that the microstructural changes are greatest in anterior brain regions and show an anterior to posterior gradient (Ardekani et al., 2007; Bhagat and Beaulieu, 2004; Head et al., 2004; Pfefferbaum et al., 2000, 2005; Pfefferbaum and Sullivan, 2003; Salat et al., 2005; Sullivan et al., 2006; Bendlin et al., in press). Although the mean diffusivity (MD) has been found to increase with age in previous studies (Abe et al., 2008; Bhagat & Beaulieu, 2004; Pfefferbaum et al., 2005; Pfefferbaum and Sullivan, 2003; Bendlin et al., in press), it did not significantly change with age in the whole brain white matter (WBWM), ROIs or VBA in this study. A possible reason for the negative MD versus age results is that the age distribution was most heavily weighted between the ages of 20 and 55, whereas the other published studies had samples that were more heavily weighted towards older individuals.

Of the diffusion tensor (DT) measures, the axial diffusivity, Da, most consistently showed age related decrease (in WBWM, CCg ROI and VBA). The VBA studies revealed age-related changes in many peripheral WM regions in frontal, parietal and occipital lobes as well as the left cerebral peduncle and left PLIC. The axial diffusivity (Da) has been suggested as a sensitive marker of axonal changes (axonal loss, injury, caliber change) (Song et al., 2003). Conversely, the radial diffusivity, Dr, a suggested marker of myelin changes (Song et al. 2002), only showed significant age related increases in the genu of the corpus callosum ROI but not in the VBA. The Dr and Da results suggest that white matter myelination is not highly affected although axonal alternations may be occurring over this age range.

The effects of age in adults on both bi-exponential diffusion and probability density function (PDF) measures have not been previously reported. For the bi-exponential model, f1 (fast diffusion fraction) decreased (and by definition the slow diffusion fraction f2 increased) and D1 (fast diffusivity) increased with age. The VBA of f1 versus age showed extensive regions of significance including areas of the prefrontal white matter, the cerebral peduncles and internal capsule, splenium of the corpus callosum, and portions of the superior longitudinal fasciculus. The spatial patterns of age-related changes in f1 are similar to the areas in the VBA of Da, although the clusters are much larger in the f1 maps. The fast diffusivity, D1, showed significant age-related changes in WBWM and CCs; however, the VBA did not reveal similar patterns. The slow diffusivity, which is a measure of more restricted diffusion, did not show any age-related changes for any of the analyses. The specific mechanisms of the bi-exponential diffusion compartments have been a subject of considerable debate (Mulkern et al., 1999; Maier et al., 2004). Some studies have suggested

that the fast and slow diffusion components are related to the extra- and intra- axonal water compartments (Assaf & Cohen, 1998; Inglis et al., 2001; Assaf & Basser 2005). Using this biological description, the results from this study suggest that the extra-axonal compartments are decreasing and/or the intra-axonal compartments are increasing with age. It is interesting that while the extra-axonal compartment appears to be decreasing, the apparent diffusivity associated with that compartment is increasing. Conversely, other studies have suggested that bi-exponential diffusion is caused even in single compartment systems with impermeable barriers (Sukstanskii et al., 2003), which would suggest that changes in f1 and D1 are induced by increased spacing of membrane of the tissues. This may reflect changes in the white matter microstructure with age that were not quite detectable with the MD measure.

The PDF measures, Po and MSD, have been studied during childhood, but not through adulthood. In children Po increases and MSD decreases with brain maturation but these trends appear to plateau during adolescence (Ben Bashat et al. 2005). In this study of aging between 18 and 72 years, neither Po nor MSD showed any significant age-related changes in WBWM or regional ROIs. However, VBA did reveal regions of significant changes in the PDF measures. Po showed age-related changes in the cerebral peduncles and transpontine WM regions. MSD appeared to increase with age in right ventrolateral prefrontal white matter, bilateral external capsule, and right temporoparietal white matter.

Po is an indicator of the most restricted or hindered diffusion although the mechanism for its modulation remains unclear. Several studies have suggested that the restricted diffusion signal from high b-values arises from the intra-axonal compartment whose water diffuses perpendicularly to fibers (Assaf & Cohen 2000). This is further supported by compelling studies of axonal measurements with high b-value DWI at different diffusion times (Assaf et al., 2008; Barazany et al., 2009). However, recent q-space imaging studies in myelin deficient rat brains and spinal cords (fixed ex vivo), and an in vivo sh pup canine model (Wu et al. 2007; 2009) suggest that changes in Po appear to be mainly modulated by myelin (Biton et al. 2006; Bar-Shir et al. 2009). Another possibility is that the restricted diffusion measure Po is modulated by the densities of barriers and membranes in the tissue, which would suggest both myelin and axonal effects as well as any other membranes. In addition, PDF measures have been shown to be sensitive to brain pathology. In a study of multiple sclerosis, Po was reduced in both lesions and normal appearing white matter (NAWM) (Assaf et al., 2005). Restricted diffusion in WM also appears reduced in patients with vascular dementia (Mayzel-Oreg et al., 2007). Higher b-value DWI experiments have also shown increased sensitivity to microstructural changes in cerebral gliomas (Seo et al., 2008) and Creutzfeldt-Jakob disease (Hyare et al., in press). Thus, the specific mechanisms of PDF measures in typical WM remain unclear. Regardless of the specific mechanisms, in this study, these measures appear to be very stable over typical adulthood.

The effects of gender on the diffusion measures appeared to be small. WBWM and ROI analyses did not reveal any significant gender differences, except increased FA in men in WBWM. The ANCOVA test showed no gender differences in the slopes of age dependence. VBA did reveal higher MSD values in left prefrontal WM in men. VBA also revealed gender differences in many diffusion measures in right occipital WM. Gender differences have been studied mostly using morphometric (Good 2001; Raz 1997; Filipek 1994; Xu 2000; Takahashi et al., in press) and DTI (Hsu et al., 2008; Szeszko et al., 2003; Oh et al., 2007; Sullivan et al., 2001; Westerhausen et al., 2004) methods. The recent voxel-based morphometry study by Takahashi et al. showed reduced gray matter volumes in left prefrontal cortex of adults less than 50 years of age, which is consistent with the increased MSD of left prefrontal white matter in men shown here. However, no previous reports have used diffusion-weighted imaging with higher b-values and only one study included axial and

radial diffusivities (Hsu et al., 2008). The reported findings of gender effects in DTI (mostly FA, few MD) have been inconsistent. Some found no gender differences (Sullivan et al., 2001), while others found significantly greater FA decreases with age in females in the deep right temporal region (Hsu et al., 2008), significantly higher FA in females in the left frontal lobe (Szeszko et al., 2003), significantly higher FA in males in the corpus callosum body, and higher FA in females in the genu and splenium of the corpus callosum (Oh et al., 2007). The increased regional FA of male subjects in this study appeared associated with decreased Dr, which is consistent with a previous study (Hsu et al. 2008) suggesting that the gender differences in DTI may be modulated by myelination. Another potential mechanism of FA gender effects includes the effects of testosterone on axonal and not myelin development during childhood and adolescence (Perrin et al., 2008).

We explored three analysis methods – global WM, ROI and VBA. The techniques for whole brain WM and ROI analysis are different from VBA so different outcomes could arise as a result. The region-of-interest methods including WBWM were performed in the native space and the latter was in the normalized standard space that required multiple imaging registration and smoothing. The WBWM analysis will be very insensitive to small and/or focal effects. In addition, global tissue segmentation may be prone to partial voluming (Pfefferbaum 2003). In this study, although we imposed a 90% threshold of the WM probability masks to minimize partial volume effects, these effects are not totally eliminated as the voxel dimensions are fairly large ($2\times2\times3$ mm). ROI studies are more anatomical specific, but require accurate manual delineation of the region, which is user dependent (Abe 2008). VBA is heavily influenced by imaging processing algorithms such as the registration algorithm (linear (affine) vs. nonlinear diffeomorphic), the type of interpolation, and the amount of smoothing. The T-SPOON VBA approach used here compensates for some of the smoothing effects from image registration (interpolation) and blurring (Lee et al., 2009). For the VBA, a linear registration algorithm (12 parameter affine transform) was used, while a nonlinear registration method might have provided greater sensitivity to more localized brain variation.

This study demonstrates that approaches like HYDI may be used to characterize different diffusion measures in a single study across a group of individuals. In addition to studies of age across a broader range, these methods could be used to investigate microstructural changes that appear to be related to specific brain function. For example, the voxel-based analyses demonstrated decreased Po with age, which may reflect a subtle decline in motor function with aging. However, no behavioral data was collected to investigate this relationship. Future studies relating HYDI measures to cognitive and behavioral performance in both healthy subjects and patients with neurological diseases may yield important insights into structure – function relationships in both the healthy and diseased brain.

One limitation of this study is that the sample sizes for older ages (over 55) is small and only includes women. Thus the results are likely to be most representative for healthy adults between 20 and 55. The limited age sampling is likely one reason that we did not observe a nonlinear (i.e., quadratic) age-dependence that other research studies have reported (Hasan et al., 2008; Lebel et al., 2010; Bendlin et al., 2010). Subjects were screened for potential health and medical conditions that may influence white matter microstructure, thus it was generally assumed that the measurements represent a healthy cohort. This evaluation of mental and physical health did not involve any clinical evaluation, but is based upon a self-report questionnaire, which may have limited accuracy. Further, this is a cross-sectional investigation that does not control for potential confounds of brain volume and other sources of individual differences like education, IQ, race, ethnicity or a family history of health-

related complications. The age- and gender-dependent observations from this study may also not reflect changes in different patient populations.

Conclusions

In this study, we characterized cerebral diffusion properties using both DTI and high b-value q-space approaches including probability density function (PDF) reconstruction and bi-exponential model fitting over a wide age range of healthy adults. The diffusion measures f1, D1 and Da were most influenced by age whereas measures of restricted, slow, and radial diffusion - Po, D2 and Dr – appear to be stable across this age range. An age-related decrease in FA was observed in prefrontal areas including the genu of the corpus callosum. Taken together, these results suggest that myelination is generally stable in most of the white matter through much of healthy adulthood; however the axonal properties may be affected.

Acknowledgments

References

Abe O, Aoki S, Hayashi N, Yamada H, Kunimatsu A, Mori H, Yoshikawa T, Okubob T, Ohtomo K. Normal aging in the central nervous system: quantitative MR diffusion-tensor analysis. Neurobiol Aging. 2002; 23:433–441. [PubMed: 11959406]

Abe O, Yamasue H, Aoki S, Suga M, Yamada H, Kasai K, Masutani Y, Kato N, Kato N, Ohtomo K. Aging in the CNS: Comparison of gray/white matter volume and diffusion tensor data. Neurobiol Aging. 2008; 29:102–116. [PubMed: 17023094]

Alexander AL, Hasan KM, Lazar M, Tsuruda JS, Parker DL. Analysis of partial volume effects in Diffusion-Tensor MRI. Magn Reson Med. 2001; 45:770–780. [PubMed: 11323803]

Alexander AL, Lee JE, Lazar M, Field AS. Diffusion Tensor Imaging of the Brain. Neurotherapeutics. 2007; 4(3):316–29. (review). [PubMed: 17599699]

Alexander DC, Barker GJ, Arridge SR. Detection and Modeling of non-gaussian apparent diffusion coefficient profiles in human brain data. Magn Reson Med. 2002; 48:331–340. [PubMed: 12210942]

Ardekani S, Kumar A, Bartzokis G, Sinha U. Exploratory voxel-based analysis of diffusion indices and hemispheric asymmetry in normal aging. Magn Reson Imaging. 2007; 25:154–167. [PubMed: 17275609]

Assaf Y, Cohen Y. Non-mono-exponential attenuation of water and N-acetyl aspartate signals due to diffusion in brain tissue. J Magn reson. 1998; 131:69–85. [PubMed: 9533908]

Assaf Y, Cohen Y. Assignment of the water slow-diffusing component in the central nervous system using q-space diffusion MRS: implications for fiber tract imaging. Magn Reson Med. 2000; 43(2): 191–199. [PubMed: 10680682]

Assaf Y, Ben Bashat D, Chapman J, Peled S, Biton IE, Kafri M, Segev Y, Hendler T, Korczyn AD, Graif M, Cohen Y. High b-value q-space analyzed diffusion-weighted MRI: application to Multiple sclerosis. Magn Reson Med. 2002; 47:115–126. [PubMed: 11754450]

Assaf Y, Chapman J, Ben-Bashat D, Hendler T, Segev Y, Korcyzn AD, Graif M, Cohen Y. White Matter Changes in Multiple Sclerosis: correlation of q-space diffusion MRI nad 1H MRS. Magn Reson Imaging. 2005; 23(6):703–710. [PubMed: 16198825]

Assaf Y, Basser PJ. Composite hindered and restricted model of diffusion (CHARMED) MR imaging of hyman brain. NeuroImage. 2005; 27:48–58. [PubMed: 15979342]

Assaf Y, Blumenfeld-Katzir T, Yovel Y, Basser PJ. AxCaliber: a method for measuring axon diameter distribution from diffusion MRI. Magn Reson Med. 2008; 59(6):1347–54. [PubMed: 18506799]

Barazany D, Basser PJ, Assaf Y. In vivo measurement of axon diameter distribution in the corpus callosum of rat brain. Brain. 2009; 132(Pt 5):1210–1220. [PubMed: 19403788]

Bar-Shir A, Duncan ID, Cohen Y. QSI and DTI od excised brain of the myelin-deficient rat. Neuroimage. 2009; 48(1):109–116. [PubMed: 19539038]

Basser PJ, Mattiello J, Le Bihan DL. Estimation of the effective self-diffusion tensor from the NMR spin echo. J Magn Reson B. 1994; 103:247–254. [PubMed: 8019776]

Basser PJ, Pierpaoli C. Microstructural and physiological features of tissues elucidated by quantitative-diffusion-tensor MRI. Magn Reson Med. 1996; 111:209–219.

Ben Bashat D, Ben Sira L, Graif M, Pianka P, Hendler Y, Cohen Y, Assaf Y. Normal White Matter Development From Infancy to Adulthood: Comparing Diffusion Tensor and High b Value Diffusion Weighted MR Images. J Magn Reson Imaging. 2005; 21:503–511. [PubMed: 15834918]

Bendlin BB, Fitzgerald ME, Ries ML, Xu G, Kastman EK, Thiel BW, Rowley HA, Lazar M, Alexander AL, Johnson SC. White Matter in Aging and Cognition: A Cross-sectional Study of Microstructure in Adults Aged Eighteen to Eighty-Three. Developmental Neuropsychology. (in press).

Bhagat YA, Beaulieu C. Diffusion Anisotropy in Subcortical White Matter and Cortical Gray Matter: Changes With Aging and the Role of CSF-Suppression. J Magn Reson Imaging. 2004; 20:216–227. [PubMed: 15269946]

Callaghan, PT. Principles of Nuclear Magnetic Resonance Microscopy. Clarendon Press; Oxford: 1991.

Biton IE, Duncan ID, Cohen Y. High b-value q-space diffusion MRI in myrlin-deficient rat spinal cords. Magn Reson Imaging. 2006; 24(2):161–166. [PubMed: 16455404]

Clark CA, Hedehus M, Moseley ME. In Vivo Mapping of the Fast and Slow Diffusion Tensor in Human Brain. Magn Reson Med communications. 2002; 47:623–628.

Cook, PA.; Bai, Y.; Nedjati-Gilani, S.; Seunarine, KK.; Hall, MG.; Parker, GJ.; Alexander, DC. Camino: Open-Source Diffusion-MRI Reconstruction and Processing. 14th Scientific Meeting of the International Society for Magnetic Resonance in Medicine; Seattle, WA, USA. 2006. p. 2759

Filipek PA, Richelme C, Kennedy DN, Caviness VS Jr. The young adult human brain: an MRI-based morphometric analysis. 1994

Good CD, Johnsrude IS, Ashburner J, Henson RNA, Friston KJ, Frackowiak RSJ. A Voxel-Based Morphometric Study of ageing in 465 Normal Adult Human Brains. NeuroImage. 2001; 4:21–36. [PubMed: 11525331]

Hasan KM, Ewing-Cobbs L, Kramer LA, Fletcher JM, Narayana PA. Diffusion tensor quantification of the macrostructure and microstructure of human midsagittal corpus callosum across the lifespan. NMR Biomed. 2008; 21:1094–1101. [PubMed: 18615857]

Head D, Buckner RL, Shimony JS, Williams LE, Akbudak E, Conturo TE, McAvoy M, Helenius J, Soinne L, Perkiö J, Salonen O, Kangasmäki A, Kaste M, Carano RAD, Aronen HJ, Tatlisumak T. Diffusion-Weighted MR Imaging in Normal Human Brains in Various Age Groups. Am J Neuroradiol. 2002; 23:194–199. [PubMed: 11847041]

Holden, RR. Holden Psychological Screening Inventory manual. North Tonawanda, NY: Multi-Health Systems; 1996.

Hsu J-L, Leemans A, Bai C-H, Lee C-H, Tsai Y-F, Chiu H-C, Chena W-H. Gender differences and age-related white matter changes of the human brain: A diffusion tensor imaging study. NeuroImage. 2008; 39:566–577. [PubMed: 17951075]

Hua K, Zhang J, Wakana S, Jiang H, Li X, Reich DS, Calabresi PA, Pekar JJ, van Zijl PCM, Mori S. Tract probability maps in stereotaxic spaces: Analysis of white matter anatomy and tract-specific quantification. NeuroImage. 2008; 39:336–347. [PubMed: 17931890]

Hugenschmidt CE, Peiffer AM, Kraft RA, Casanova R, Deibler AR, Burdette JH, Maldjian JA, Laurienti PJ. Relating Imaging Indices of White Matter Integrity and Volume in Healthy Older Adults. Cereb Cortex. 2008; 18(2):433–42. [PubMed: 17575289]

Hyare H, Thornton J, Stevens J, Mead S, Rudge P, Collinge J, Yousry TA, Jager HR. High-b-value Diffusion MR Imaging and Basal Nuclei Apparent Diffusion Coefficient Measurements in Variant and Sporadic Creutzfeldt-Jakob Disease. Am J Neuroradiol. in press.

Inglis BA, Bossart EL, Buckley DL, Wirth ED III, Mareci TH. Visualization of Neural Tissue Water Compartmentts Using Biexponential Diffusion Tensor MRI. Magn Reson Med. 2001; 45:580–587. [PubMed: 11283985]

Jenkinson M, Smith SM. A global optimisation method for robust affine registration of brain images. Medical Image Analysis. 2001; 5(2):143–156. [PubMed: 11516708]

Lebel C, Caverhill-Godkewitsch S, Beaulieu C. Age-related regional variations of the corpus callosum identified by diffusion tensor tractography. NeuroImage. 2010 April.

Lee JE, Moo CK, Lazar M, DuBray MB, Kim J, Bigler ED, Lainhart JE, Alexander AL. A study of diffusion tensor imaging by tissue-specific, smoothing-compensated voxel-based analysis. NeuroImage. 2009; 44:870–883. [PubMed: 18976713]

Maier SE, Bogner P, Bajzik G, Mamata H, Mamata Y, Repa I, Jolesz FA, Mulkern RV. Normal Brain and Brain Tumor: Multicomponent Apparent Difusion Coefficient Line Scan Imaging. Radiology. 2001; 219:842–849. [PubMed: 11376280]

Maier SE, Vajapeyam S, Mamata H, Westin C-F, Jolesz FA, Mulkern RV. Biexponential Diffusion Tensor Analysis of Human Bairn Diffusion Data. Magn Reson Med. 2004; 51:321–330. [PubMed: 14755658]

Mayzel-Oreg O, Assaf Y, Gigi A, Ben-Bashat D, Verchovsky R, Mordohovitch M, Graif M, Hendler T, Korczyn A, Cohen Y. High b-value diffusion imaging of dementia: application to vascular dementia and Alzheimer disease. J Neurol Sci. 2007; 15(257):105–113. [PubMed: 17360001]

Mori, S.; Wakana, S.; Nagae-Poetscher, LM.; van, ZijlPCM. MRI Atlas of Human White Matter. Elsevier; Amsterdam, The Netherlands: 2005.

Mulkern RV, Gudbjartsson H, Westin C-F, Zengingonul HP, Gartner W, Guttmann CRG, Robertson RL, Kyriakos W, Schwartz R, Holtzman D, Jolesz FA, Maier SE. Multi-component apparent diffusion coefficients in human brain. NMR Biomed. 1999; 12:51–62. [PubMed: 10195330]

Nichols TE, Holmes AP. Nonparametric Permutation Tests for Functional Neuroimaging: A Primer with Examples. Human Brain Mapping. 2002; 15:1–25. [PubMed: 11747097]

Perrin JS, Herve P, Leonard G, Perron M, Pike GB, Pitiot A, Richer L, Veillette S, Pausova Z, Paus T. Growth of white matter in the adolescent brain: Role of testosterone and androgen receptor. J Neurosci. 2008; 28:9519–9524. [PubMed: 18799683]

Pierpaoli C, Basser PJ. Toward a Quantitative Assessment of Diffusion Anisotropy. Magn Reson Med. 1996; 36:893–906. [PubMed: 8946355]

Pfefferbaum A, Sullivan EV, Hedehus M, Lim KO, Adalsteinsson EA, Moseley M. Age-Related Decline in Brain White Matter Anisotropy Measured With Spatially Corrected Echo-Planar Diffusion Tensor Imaging. Magn Reson Med. 2000; 44:259–268. [PubMed: 10918325]

Pfefferbaum A, Sullivan EV. Increased Brain White Matter Diffusivity in Normal Adult Aging: Relationship to Anisotropy and Partial Voluming. Magn Reson Med. 2003; 49:953–961. [PubMed: 12704779]

Pfefferbaum A, Adalsteinsson E, Sullivan EV. Frontal circuitry degradation marks healthy adult aging: Evidence from diffusion tensor imaging. NeuroImage. 2005; 26:891–899. [PubMed: 15955499]

Oh, Js; Song, IC.; Lee, Js; Kang, H.; Park, KS.; Kang, E.; Lee, DS. Tractography-guided statistics (TGIS) in diffusion tensor imaging for the detection of gender difference of fiber integrity in the midsagittal and parasagittal corpora callosa. NeuroImage. 2007; 36:606–616. [PubMed: 17481923]

Raz N, Gunnubg FM, Head D, Dupuis JH, McQuain J, Briggs SD, Loken WJ, Thornton AE, Acker JD. Selective Aging of the Human Cerebral Cortex Observed in Vivo: Differential Vulnerability of the Prefrontal Gray Matter. Cerebral Cortex. 1997; 7:268–282. [PubMed: 9143446]

Salat DH, Tuch DS, Greve DN, van der Kouwe AJW, Hevelone ND, Zaleta AK, Rosen BR, Fischl B, Corkin S, Rosas HD, Dale AM. Age-related alterations in white matter microstructure measured by diffusion tensor imaging. Neurobiol Aging. 2005; 26:1215–1227. [PubMed: 15917106]

Seo HS, Chang KH, Na DG, Kwon BJ, Lee DH. High b-value diffusion (b = 3000 s/mm^2) MR imaging in cerebral gliomas at 3T: visual and quantitative comparisons with b = 1000 s/mm^2. Am J Neuroradiol. 2008; 29(3):458–463. [PubMed: 18065512]

Smith SM, Nichols TE. Threshold-free cluster enhancement: Addressing problems of smoothing, threshold dependence and localisation in cluster inference. NeuroImage. 2009; 44(1):83–98. [PubMed: 18501637]

Song SK, Sun S-W, Ramsbottom MJ, Chang C, Russell J, Cross AH. Dysmyelintaion revealed through MRI as increased radial (but unchanged axial) diffusion of water. NeuroImage. 2002; 17:1429–1436. [PubMed: 12414282]

Song SK, Sun S-W, Ju W-K, Lin S-J, Cross AH, Neufeld AH. Diffusion tensor inaging setects and differentiates axon and myelin degeneration in mouse optic nerve after retinal ischemia. NeuroImage. 2003; 20:1714–1722. [PubMed: 14642481]

Sukstanskii AL, Ackerman JJH, Yablonsky DA. Effects of barrier-induced nuclear spin magnetization inhomogeneities on diffusion-attenuated MR signal. Magn Reson Med. 2003; 50:735–742. [PubMed: 14523959]

Sullivan EV, Adalsteinsson E, Hedehus M, Ju C, Moseley M, Lim KO, Pfefferbaum A. Equivalent distribution of regional white matter microstructure in aging healthy men and women. NeuroReport. 2001; 12:99–104. [PubMed: 11201100]

Sullivan EV, Adalsteinsson E, Pfefferbaum A. Selective age-related degradation of anterior callosal fiber bundles quantified in vivo with fiber tracking. Cerebral Cortex. 2006; 16(7):1030–1039. [PubMed: 16207932]

Szeszko PR, Vogel J, Ashtari M, Malhotra AK, Bates J, Kane JM, Bilder RM, Frevert T, Lim K. Sex diferences in frontal lobe white matter microstructure: a DTI study. NeuroReport. 2003; 14(18):2469–2473. [PubMed: 14663212]

Takahasi R, Ishii K, Kakigi T, Yokoyama K. Gender and age differences in normal adult human brain: voxel-based morphometry study. Human Brain Mapping. in press.

Tofts, P. Quantitative MRI of the Brain. John Wiley & Sons Ltd; England: 2003. p. 217

Wedeen VJ, Hagmann P, Tseng W-YJ, Reese TG, Weisskoff RM. Mapping complex tissue architecture with diffusion spectrum magnetic resonance imaging. Magn Reson Med. 2005; 54:1377–1386. [PubMed: 16247738]

Voineskos AN, Lobaugh NJ, Bouix S, Rajji TK, Miranda D, Kennedy JL, Mulsant BH, Pollock BG, Shenton ME. Diffusion tensor tractography findings in schizophrenia across the adult lifespan. Brain. (in press).

Wu Y-C, Alexander AL. Hybrid diffusion imaging. NeuroImage. 36:617–629. [PubMed: 17481920]

Wu Y-C, Field AS, Alexander AL. Computation of Diffusion Function Measures in q-Space Using Magnetic Resonance Hybrid Diffusion Imaging. IEEE Trans Med Imaging. 2008; 27(6):858–865. [PubMed: 18541492]

Wu, Y-C.; Alexander, AL.; Duncan, ID.; Field, AS. Hybrid diffusion imaging in a brain model of dysmyelination. Proc. ISMRM-ESMRMB Joint Annual meeting; Berlin, Germany. 2007. p. 73-318.

Wu, Y-C.; Alexander, AL.; Duncan, ID.; Field, AS. Hybrid Diffusion Imaging (HYDI) in a Brain Model of Dysmyelination. Proc. ISMRM 17th Annual meeting; Honolulu, Hawaii. 2009. p. 157-739.

Xu J, Kobayashi S, Yamahuchi S, Iijima K-i, Okada K, Yamashita K. Gender Effects on Age-Related Changes in Brain Structure. AJNR. 2000; 21:112–118. [PubMed: 10669234]

Zhang Y, Brady M, Smith S. Segmentation of brain MR images through a hidden Markov random field model and the expectation maximization algorithm. IEEE Trans on Medical Imaging. 2001; 20(1):45–57.
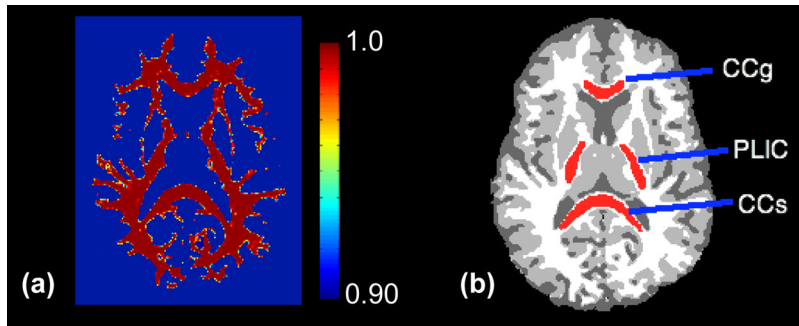
Figure 1.
Example white matter mask and ROIs. (a) White matter (WM) probability mask with color scales denoting classification probability. (b) Tissue segmentation on Po map. White: WM, Gray: gray matter (GM) and dark gray: cerebrospinal fluid (CSF). Red: ROIs, from anterior to posterior: genu of the corpus callosum (CCg), posterior limbs of bilateral internal capsules (PLIC) and splenium of the corpus callosum (CCs). ROIs are all three-dimensional and cover four consecutive slices. The original Po map of the same subject is in Figure 2 (a).
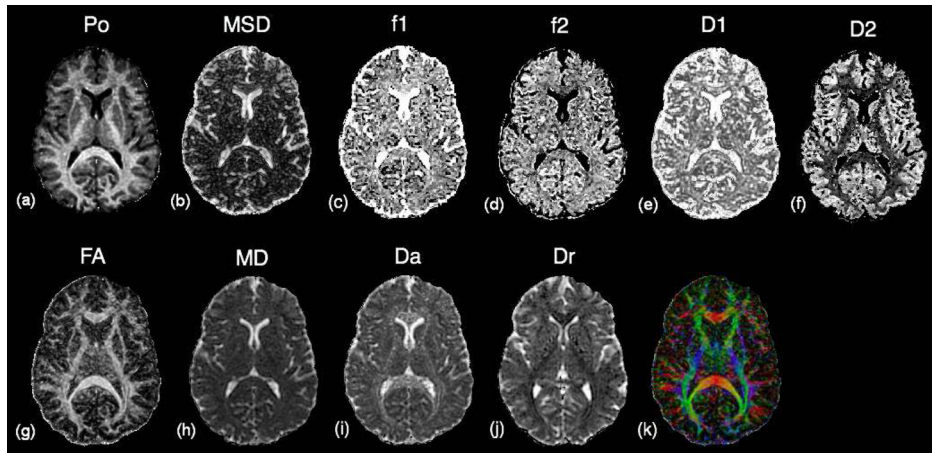
Figure 2.
Maps of diffusion-weighted (DW) measures of a 26 year old male subject in HYDI experiment. From the whole dataset, PDF measures: (a) Po, zero displacement probability, a measure of tissue restriction; (b) MSD, mean squared displacement, a measure of averaged diffusivity. Bi-exponential model fitting of the whole dataset: (c) f1, the volume fraction of the fast diffusion compartment; (d) f2, the volume fraction of the slow diffusion compartment; (e) D1, averaged diffusivity of the fast compartment; (f) D2, averaged diffusivity of the slow compartment. DTI measures from inner shell: (g) FA, fractional anisotropy of diffusion tensor (DT) model; (h) MD, mean diffusivity of DT model; (i) Da, axial diffusivity, (j) Dr, radial diffusivity, and (k) major eigenvector colormap.
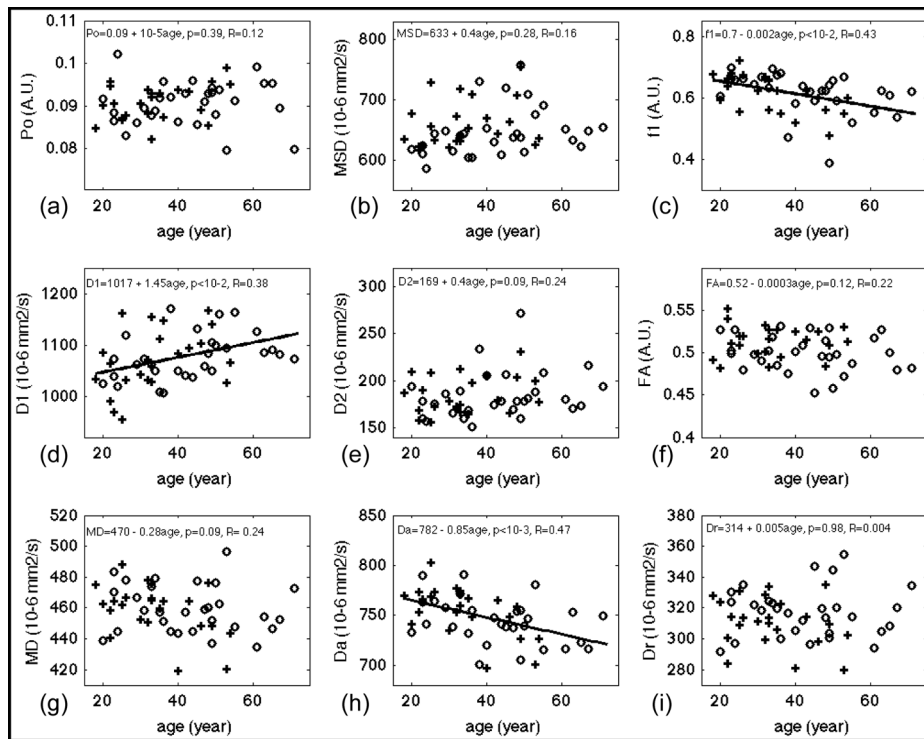
Figure 3.
Results of linear regression of diffusion measures versus age for whole-brain white matter. PDF measures: (a) Po, zero displacement probability; (b) MSD, mean squared displacement, a measure of averaged diffusivity using Einstein diffusion equation. Bi-exponential model fitting of the whole dataset: (c) f1, the volume fraction of the fast diffusion compartment; (d) D1, averaged diffusivity of the fast compartment; (e) D2, averaged diffusivity of the slow compartment. DTI measures from inner shell: (f) FA, fractional anisotropy; (g) MD, mean diffusivity; (h) Da, axial diffusivity, (i) Dr, radial diffusivity. Gender effect if significant has been corrected from these plots. Regression lines were plotted only for measures with significant fit, i.e. $p < 0.05$. Fitted equations are shown on top of each panel, where the linear model was DW measure = constant + β_1*age + error, p, i.e. p-value, denotes the significance of fit and R denotes the correlation coefficient. Cross (+) and circle (○) denotes averaged diffusion measurements at that age for male and female respectively. A.U. denotes arbitrary unit.

Figure 4.
Results of linear regression of diffusion measures versus age for ROI at the genu of corpus callosum (CCg). PDF measures (a) Po; (b) MSD. Bi-exponential model fitting of the whole dataset: (c) f1; (d) D1; (e) D2. DTI measures from inner shell: (f) FA; (g) MD; (h) Da; (i) Dr. Gender effect if significant has been corrected from these plots. Regression lines were plotted only for measures with significant fit, i.e. p < 0.05. Fitted equations are shown on top of each panel, where the linear model was DW measure = constant + β_1*age + error, p, i.e. p-value, denotes the significance of fit and R denotes the correlation coefficient. Cross (+) and circle (○) denotes averaged diffusion measurements at that age for male and female respectively. A.U. denotes arbitrary unit.
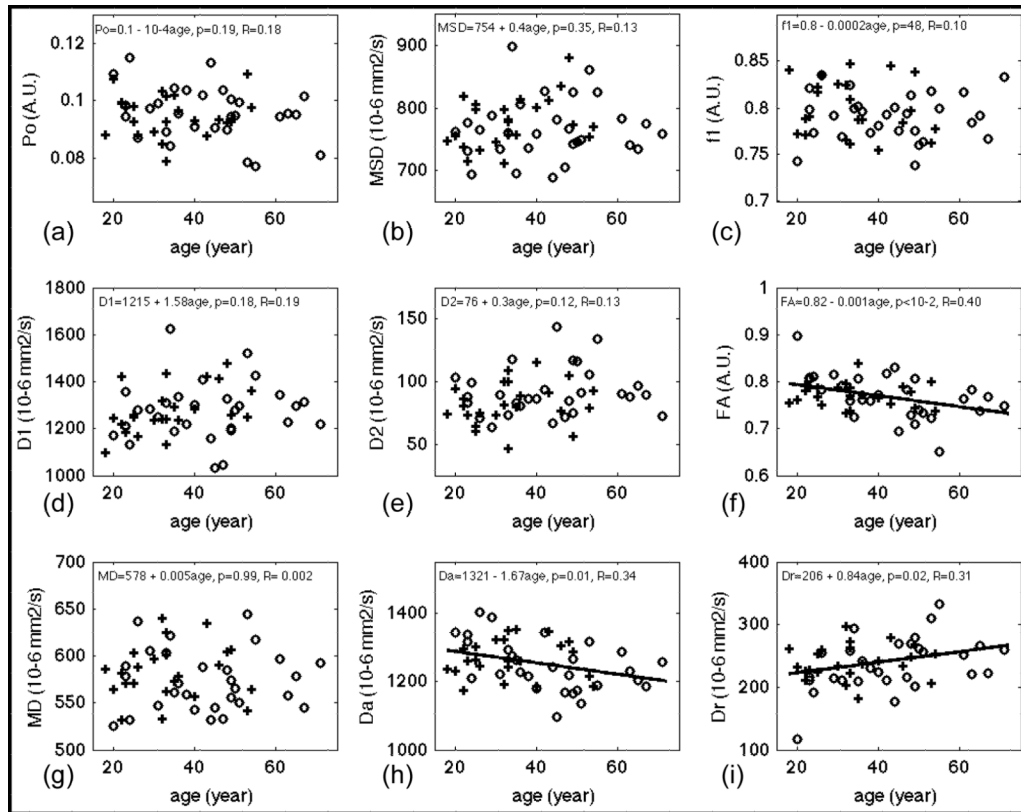
Figure 5.
Results of linear regression of diffusion measures versus age for ROI at the posterior limbs of the internal capsule (PLIC). PDF measures (a) Po; (b) MSD. Bi-exponential model fitting of the whole dataset: (c) f1; (d) D1; (e) D2. DTI measures from inner shell: (f) FA; (g) MD; (h) Da; (i) Dr. Gender effect if significant has been corrected from these plots. Fitted equations are shown on top of each panel, where the linear model was DW measure = constant + β_1*age + error, p, i.e. p-value, denotes the significance of fit and R denotes the correlation coefficient. Cross (+) and circle (○) denotes averaged diffusion measurements at that age for male and female respectively. A.U. denotes arbitrary unit.
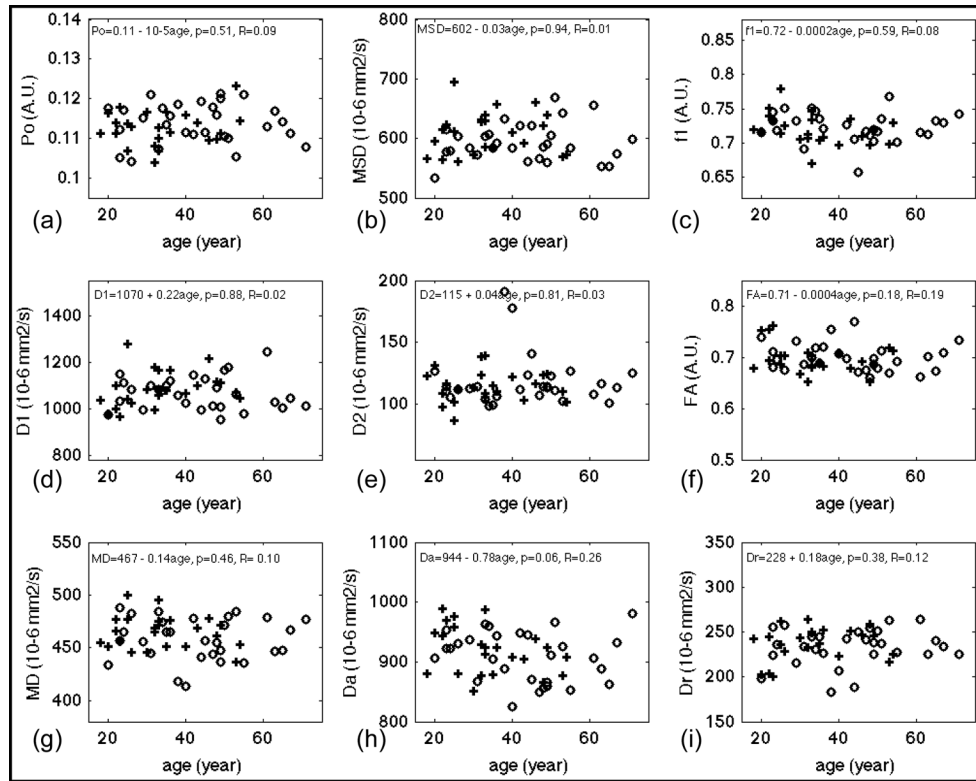
Figure 6.
Results of linear regression of diffusion measures versus age for ROI at the splenium of corpus callosum (CCs). PDF measures (a) Po; (b) MSD. Bi-exponential model fitting of the whole dataset: (c) f1; (d) D1; (e) D2. DTI measures from inner shell: (f) FA; (g) MD; (h) Da; (i) Dr. Gender effect if significant has been corrected from these plots. Regression lines were plotted only for measures with significant fit, i.e. $p < 0.05$. Fitted equations are shown on top of each panel, where the linear model was DW measure = constant + β_1*age + error, p, i.e. p-value, denotes the significance of fit and R denotes the correlation coefficient. Cross (+) and circle (○) denotes averaged diffusion measurements at that age for male and female respectively. A.U. denotes arbitrary unit.
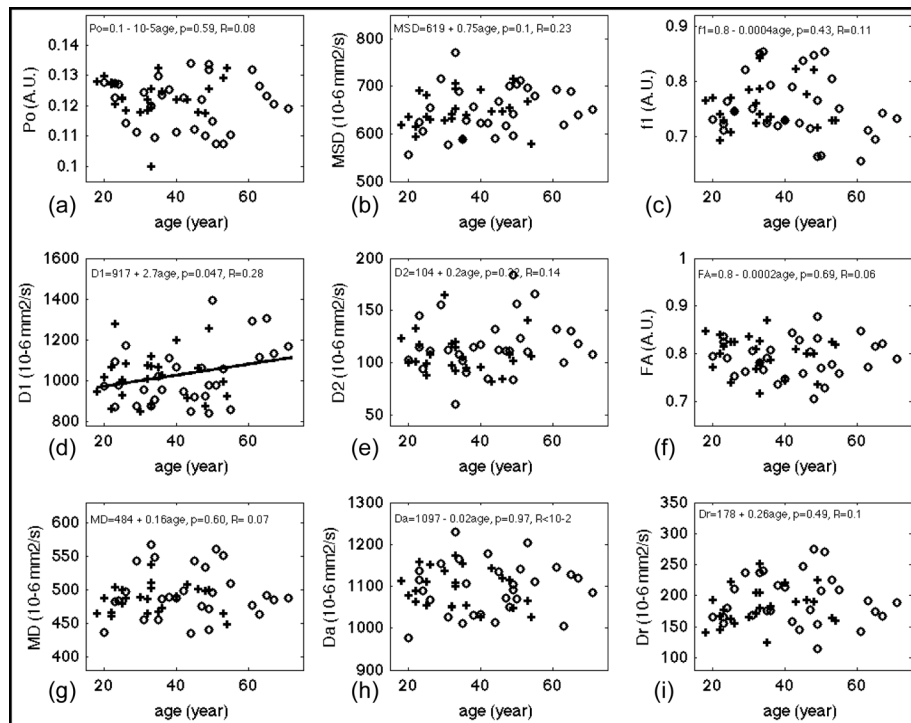
Figure 7.
Voxel based significance maps of the Po change with age. Image orientation is in radiologic convention. Notations: Red-yellow colorbar: positive correlation with age; color scale: T score; z: MNI space z coordinate in mm.

Figure 8.
Voxel based significance maps of the MSD change with age. Image orientation is in radiologic convention. Notations: Red-yellow colorbar: positive correlation with age; color scale: T score; z: MNI space z coordinate in mm.

Figure 9.
Voxel based significance maps of the f1 change with age. Image orientation is in radiologic convention. Notations: Blue-Lightblue colorbar: negative correlation with age; color scale: T score; z: MNI space z coordinate in mm.
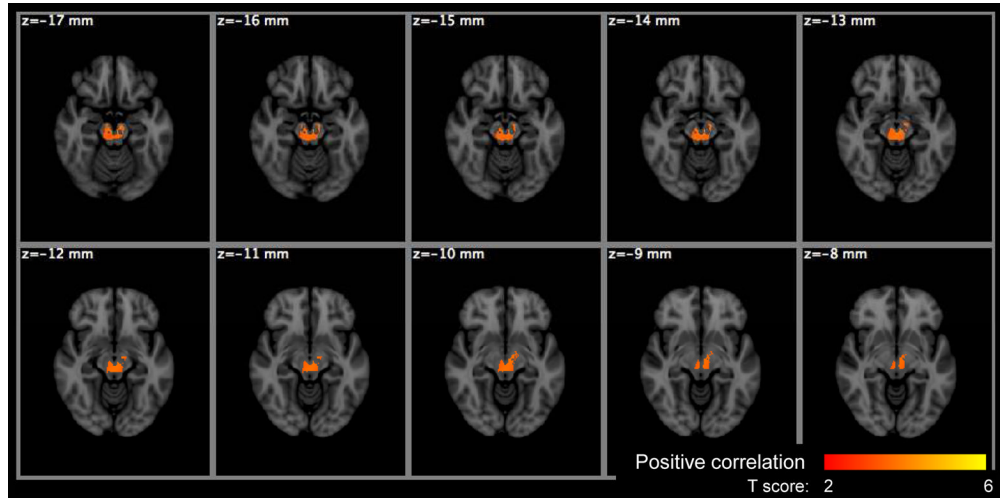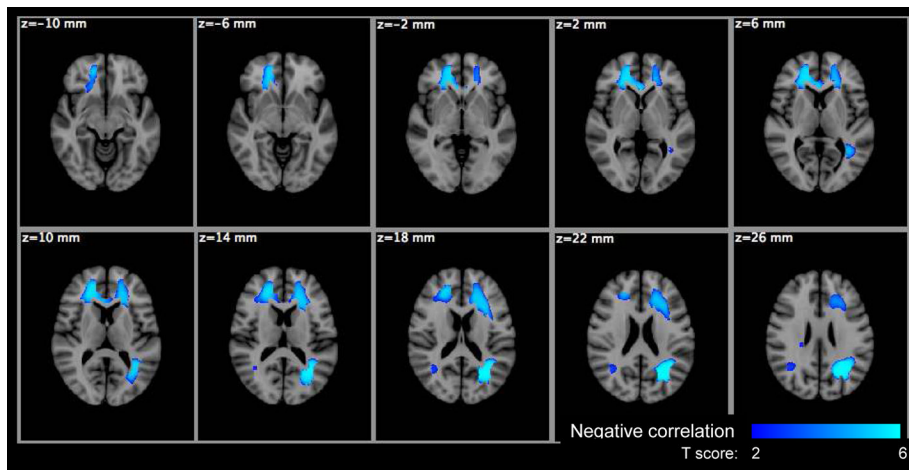
Figure 10.
Voxel based significance maps of the FA change with age. Image orientation is in radiologic convention. Notations: Blue-Lightblue colorbar: negative correlation with age; color scale: T score; z: MNI space z coordinate in mm.
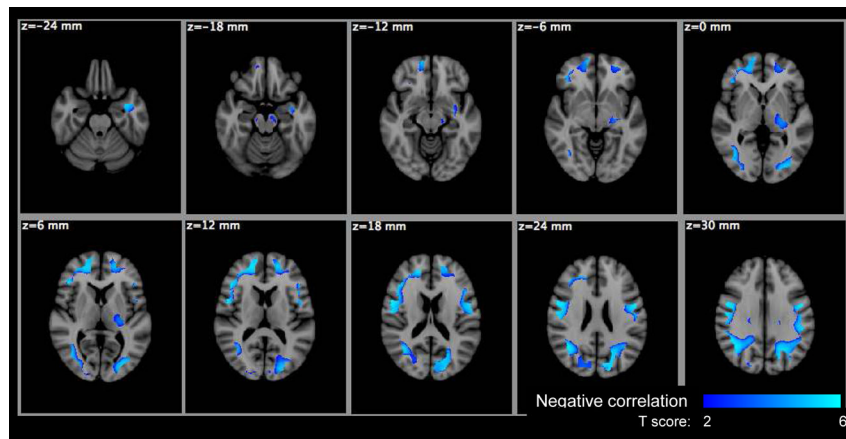
Figure 11.
Voxel based significance maps of the Da change with age. Image orientation is in radiologic convention. Notations: Blue-Lightblue colorbar: negative correlation with age; color scale: T score; z: MNI space z coordinate in mm.
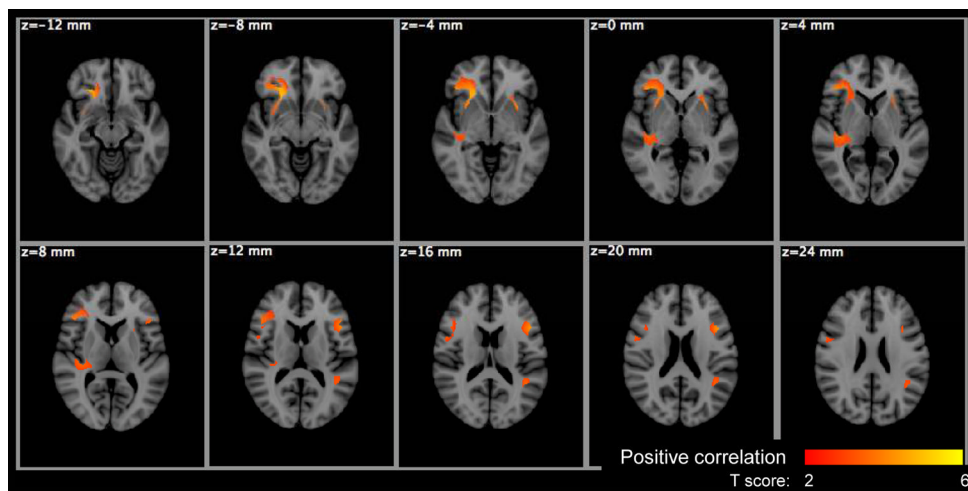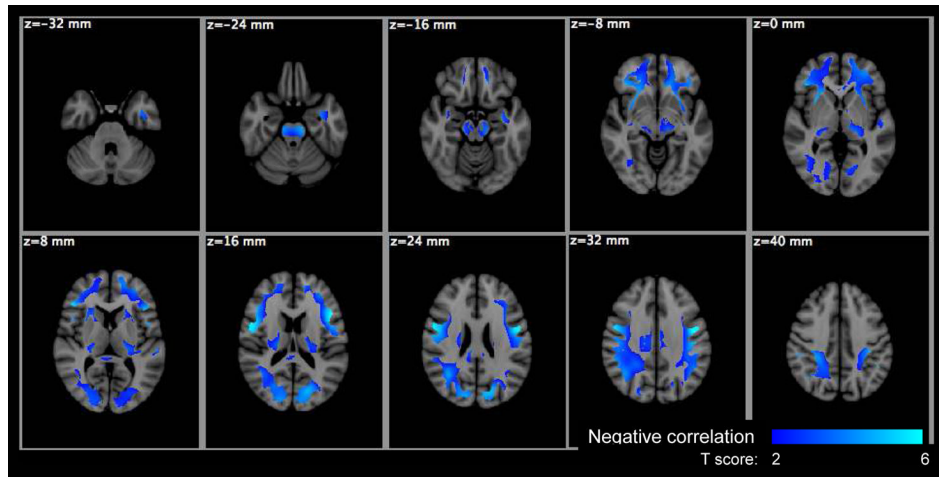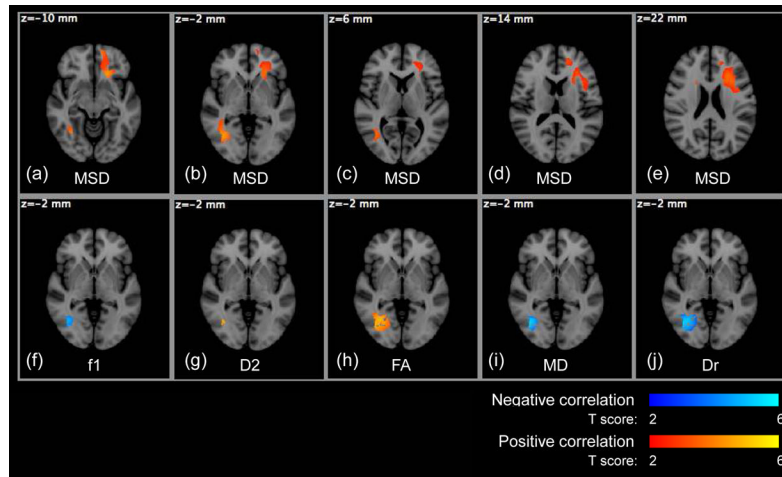
Figure 12.
Voxel based significance maps of the changes of MSD (a)–(e), f1 (f), D2 (g), FA (h), MD (i) and Dr (j) with gender (female: 0 and male: 1). Image orientation is in radiologic convention. Notations: Red-Yellow: positive correlation with gender (high in male and low in female); Blue-Lightblue colorbar: negative correlation with gender (low in male and high in female); color scale: T score; z: MNI space z coordinate in mm.

Table 1

HYDI acquisition scheme.

HYDI Shell	Ne	b value (s/mm^2)
	1	0
1st	6	375
2nd	21	1500
3rd	24	3375
4th	24	6000
5th	50	9375
total	126	

Ne denotes the number of diffusion gradient encoding directions.

Table 2

Mean values of diffusion measures across all subjects (mean±SD) for whole brain white matter and 3-dimensional ROI's.

Tissue		MSD (10^{-6}s/mm^2)	Po	f_1	f_2	D_1 (10^{-6}s/mm^2)	D_2 (10^{-6}s/mm^2)	FA	MD (10^{-6}s/mm^2)	Da (10^{-6}s/mm^2)	Dr (10^{-6}s/mm^2)
WBWM	mean ± SD	652 ± 40	0.091 ± 0.005	0.616 ± 0.065	0.384 ± 0.065	1074 ± 51	185 ± 23	0.506 ± 0.021	459 ± 16	749 ± 24	314 ± 16
CCg	mean ± SD	771 ± 45	0.096 ± 0.008	0.795 ± 0.027	0.205 ± 0.027	1276 ± 113	88 ± 19	0.771 ± 0.040	578 ± 31	1255 ± 67	239 ± 36
PLIC	mean ± SD	600 ± 34	0.113 ± 0.005	0.715 ± 0.039	0.285 ± 0.039	1074 ± 73	116 ± 18	0.699 ± 0.28	461 ± 18	914 ± 41	235 ± 20
CCs	mean ± SD	649 ± 44	0.122 ± 0.008	0.755 ± 0.050	0.245 ± 0.050	1022 ± 133	113 ± 23	0.795 ± 0.039	491 ± 31	1096 ± 54	188 ± 36

Notations:

WBWM: whole brain white matter;

CCg: genu of corpus callosum;

PLIC: posterior limbs of internal capsule;

CCs: splenium of corpus callosum;

SD: standard deviation across subjects regardless age and gender differences.

Table 3

Results of linear regression analysis vs. age for whole brain white matter and 3-dimensional ROI's.

Tissue		Po	MSD	f_1	f_2	D_1	D_2	FA	MD	Da	Dr
WBWM	β_1	1×10^{-5}	0.400	**−0.002**	**0.002**	**1.447**	0.401	-3×10^{-4}	−0.279	**−0.848**	0.005
	R	0.121	0.157	**0.426**	**0.426**	**0.382**	0.237	0.218	0.236	**0.475**	0.004
	p-value	0.391	0.278	**0.002**	**0.002**	**0.005**	0.091	0.121	0.093	**$<10^{-3}$**	0.976
CCg	β_1	-1×10^{-4}	0.441	-2×10^{-4}	2×10^{-4}	1.580	0.302	**−0.001**	0.005	**−1.667**	**0.841**
	R	0.183	0.132	0.100	0.100	0.189	0.128	**0.404**	0.002	**0.336**	**0.313**
	p-value	0.194	0.352	0.479	0.479	0.179	0.120	**0.003**	0.988	**0.015**	**0.024**
PLIC	β_1	3×10^{-5}	−0.028	-2×10^{-4}	2×10^{-4}	0.224	0.044	-4×10^{-4}	−0.141	−0.783	0.180
	R	0.094	0.011	0.077	0.077	0.021	0.033	0.188	0.104	0.258	0.125
	p-value	0.506	0.937	0.588	0.588	0.882	0.812	0.183	0.462	0.064	0.222
CCs	β_1	-4×10^{-5}	0.750	-4×10^{-4}	4×10^{-4}	**2.709**	0.245	-2×10^{-4}	0.165	−0.019	0.262
	R	0.077	0.231	0.112	0.112	**0.277**	0.142	0.057	0.074	0.005	0.099
	p-value	0.586	0.099	0.428	0.428	**0.047**	0.316	0.687	0.602	0.974	0.485

Bold font indicates measures with significant fit against age with p < 0.05.

Notations:

WBWM: whole brain white matter;

CCg: genu of corpus callosum;

PLIC: posterior limbs of internal capsule;

CCs: splenium of corpus callosum;

β_1: regression coefficient, the slope or the rate of the change of diffusion measure per year.

R: correlation coefficient

Table 4

Voxel based analysis of HYDI measures using permutation methods (randomization method) with age and gender as confound regressors.

	p-value (FWE- corrected)	Cluster size (voxels)	MNI coordinate (mm)			Anatomical Location
			x	y	z	
Po	*Age: Positive correlation*					
	0.037	2529	−4	−21	−16	Anterior thalamic radiation/Brain-Stem
MSD	*Age: Positive correlation*					
	0.015	7612	23	27	−7	R. Anterior corona radiata/Inferior fronto-occipital fasciculus
	0.043	2418	40	−23	2	R. Retrolenticular part of internal capsule/Inferior fronto-occipital fasciculus
	0.036	1449	−45	16	21	L. Superior longitudinal fasciculus
	0.047	1382	−42	−49	16	L. Superior longitudinal fasciculus (temporal part)
	0.043	574	−30	13	−1	L. external capsule
	Gender: Positive correlation					
	0.022	19057	−19	25	−9	L. Anterior corona radiata/Inferior fronto-occipital fasciculus/Superior longitudinal fasciculus
	0.022	4114	35	−64	−5	R. Inferior longitudinal fasciculus/Inferior fronto-occipital fasciculus
	0.040	1663	15	15	30	R. Superior corona radiata
f1	*Age: Negative correlation*					
	0.002	72262	55	2	17	R. Superior longitudinal fasciculus/Anterior corona radiata/inferior fronto-occipital fasciculus/inferior longitudinal fasciclus/cortical spinal tract/brain stem
	0.001	44397	−51	−3	33	L. Superior longitudinal fasciculus/Anterior corona radiata/inferior fronto-occipital fasciculus
	Gender: Negative correlation					
	0.028	1375	38	−65	−5	R. Inferior longitudinal fasciculus
D2	*Gender: Positive correlation*					
	0.041	361	38	−65	−5	R. Inferior longitudinal fasciculus

Notations: FWE: family wise error; MNI: Montreal Neurological Institute; Po: zero displacement probability; MSD: mean squared diffusivity; f1: volume fraction of fast diffusion compartment; D1: diffusivity of the fast diffusion compartment; D2: diffusivity of the slow diffusion compartment. The voxel size here referred the voxel size in the normalized space (MNI space), which is $1 \times 1 \times 1$ mm^3. The anatomical locations were based on the ICBM-DTI-81 white-matter labels atlas (Mori et al., 2005) and JHU white-matter tractography atlas (Hua et al., 2008) provided by FMRIB Software Library (FSL).

Table 5

Voxel based analysis of DTI measures using permutation methods (randomization method) with age and gender as confound regressors.

	p-value (FWE-corrected)	Cluster size (voxels)	MNI coordinate (mm)			Location
			x	y	z	
FA	*Age: Negative correlation*					
	0.006	25816	20	38	6	L. R. Anterior corona radiata/genu of corpus callosum/L. superior longitudinal fasciculus
	0.001	17649	−25	−62	23	L. Superior and posterior corona radiata/Superior and inferior longitudinal fasciculus/optic radiation
	0.017	2506	21	−23	35	R. Superior and posterior corona radiata
	0.04	1239	38	−57	21	R. Superior longitudinal fasciculus
	Gender: Positive correlation					
	0.006	5044	38	−68	−8	R. Inferior longitudinal fasciculus
MD	*Gender: Negative correlation*					
	0.015	2563	40	−67	−2	R. Inferior longitudinal fasciculus
Da	*Age: Negative correlation*					
	0.003	33742	54	6	18	R. Superior and posterior corona radiata/R. anterior thalamic radiation/Inferior fronto- occipital fasciculus/Superior and inferior longitudinal fasciculus/optic radiation
	0.004	25003	−53	0	26	L. Superior and posterior corona radiata/Inferior fronto-occipital fasciculus/Superior longitudinal fasciculus/
	0.014	4045	−20	52	12	L. Forceps minor
	0.028	2933	−26	−20	0	L. Posterior limb of internal capsule/L. cerebral peduncle
	0.008	1612	−36	0	−29	L. external capsule/Inferior logitudinal fasciculus/
Dr	*Gender: Negative correlation*					
	0.007	4453	38	−66	−5	R. Inferior longitudinal fasciculus

Notations: FWE: family wise error; MNI: Montreal Neurological Institute; FA: fractional anisotropy; MD: mean diffusivity; Da: axial diffusivity; Dr: radial diffusivity. The voxel size here referred the voxel size in the normalized space (MNI space), which is $1 \times 1 \times 1$ mm^3. The anatomical locations were based on the ICBM-DTI-81 white-matter labels atlas (Mori et al., 2005) and JHU white-matter tractography atlas (Hua et al., 2008) provided by FMRIB Software Library (FSL).